

Estimating air quality co-benefits of energy transition using machine learning

Da Zhang^{1,2}, Qingyi Wang³, Shaojie Song⁴, Simiao Chen^{5,6}, Mingwei Li⁷, Lu Shen⁴, Siqu Zheng⁸, Bofeng Cai^{9,*}, Shenhao Wang^{8,10,*}

- 1 Institute of Energy, Economy, and Environment, Tsinghua University, Beijing, China
- 2 Joint Program on the Science and Policy of Global Change, Massachusetts Institute of Technology, Cambridge, MA, USA
- 3 Department of Civil and Environmental Engineering, Massachusetts Institute of Technology, Cambridge, MA, USA
- 4 School of Engineering and Applied Sciences, Harvard University, Cambridge, MA, USA
- 5 Heidelberg Institute of Global Health, Faculty of Medicine and University Hospital, Heidelberg University, Heidelberg, Germany
- 6 Chinese Academy of Medical Sciences and Peking Union Medical College, Beijing, China
- 7 Center for Policy Research on Energy and the Environment, Princeton University, Princeton, NJ, USA
- 8 Department of Urban Studies and Planning, Massachusetts Institute of Technology, Cambridge, MA, USA
- 9 Center for Climate Change and Environmental Policy, Chinese Academy for Environmental Planning, Beijing, China
- 10 Media Lab, Massachusetts Institute of Technology, Cambridge, MA, USA, 02139

* To whom correspondence should be addressed. E-mail: shenhao@mit.edu and caibf@caep.org.cn.

Abstract

Estimating health benefits of reducing fossil fuel use from improved air quality provides important rationales for carbon emissions abatement. Simulating pollution concentration is a crucial step of the estimation, but traditional approaches often rely on complicated chemical transport models that require extensive expertise and computational resources. In this study, we develop a novel and succinct machine learning framework that is able to provide precise and robust annual average fine particle (PM_{2.5}) concentration estimations directly from a high-resolution fossil energy use data set. The accessibility and applicability of this framework show great potentials of machine learning approaches for integrated assessment studies. Applications of the framework with Chinese data reveal highly heterogeneous health benefits of reducing fossil fuel use in different sectors and regions in China with a mean of \$34/tCO₂ and a standard deviation of \$84/tCO₂. Reducing rural and residential coal use offers the highest co-benefits with a mean of \$360/tCO₂. Our findings prompt careful policy designs to maximize cost-effectiveness in the transition towards a carbon-neutral energy system.

The use of fossil fuel is well known as the major source of both greenhouse gas (GHG) and air pollutant emissions in most nations. Emissions abatement from fossil-fuel use reduction therefore could bring significant health benefits while addressing climate change¹⁻⁹. Understanding the heterogeneity of local health benefits from marginal emissions reductions is crucial for designing co-control abatement activities. To obtain the geographical distribution of benefits with high resolution, it usually requires adjoint¹⁰, or more commonly, reduced-form chemical transport models (CTMs) that can be iterated many times to simulate air quality changes¹¹⁻¹⁵. These reduced-form air quality models, e.g., the Air Pollution Emission Experiments and Policy analysis model (APEEP)¹⁶ and its updated versions (AP2/AP3), the Estimating Air quality Social Impacts Using Regression (EASIUR)¹⁷, the Intervention Model for Air Pollution (InMAP)¹⁸, and the TM5-Fast Scenario Screening Tool (TM5-FASST)¹⁹, often rely on linearized representations of emissions-concentration sensitivity derived from full-scale CTMs.

Although reduced-form models provide satisfying approximations for full-scale models, several important limitations restrict their use in policy analysis. First, inputs for the reduced-form model that are developed from the full-scale model (usually for a specific simulation period) are still resource-intensive, hence updating the meteorological conditions that dictate the simulation results requires substantial domain knowledge and efforts. Second, for regions where the atmospheric chemistry processes are less well understood, especially the developing nations, the biases embodied in the full-scale model will be inherited by the reduced-form model, hence affecting the accuracy of policy simulations. Third, similar to the full-scale model, the reduced-form model also needs a detailed list of emissions inventory for all the pollutant species as inputs, so strong assumptions may have to be imposed to convert fossil fuel use data to emissions inventory. To address these limitations, in this paper, we develop a machine-learning framework that is able to provide precise and robust annual average fine particle ($PM_{2.5}$) concentration estimations directly from high-resolution fossil energy use data and some additional geographic information. We apply this framework with data from China and estimate health benefits of reducing fossil fuel use in different sectors and regions. The framework is transparent, easy-to-update, and ready to be extended to other nations without establishing sophisticated full-scale CTMs.

Our framework also supplements the growing literature that applies machine learning approaches to study air-quality-related topics. Several studies have exploited the strong data-fitting capacity of machine learning methods to predict short-term pollutant concentrations. For example, Ong et al.²⁰ use a deep recurrent neural network (DRNN) to predict next 12-hour $PM_{2.5}$ concentrations in 52 Japanese cities; Kerckhoffs et al.²¹ compare performances of different machine learning methods (e.g., bagging and random forest) to predict average of three 24-h measurements of ultrafine particles (UFP) using mobile and short-term stationary measurements in Dutch cities; Xing et al.²² develop a deep-learning-based response surface model (DeepRSM) that is trained using the Community Multiscale Air Quality (CMAQ) simulations on domains that cover China to characterize the response of O_3 and $PM_{2.5}$ concentrations to emissions changes; Kelp et al.²³ discuss the design of stable, general machine-learned models of the atmospheric chemical system. There are also studies^{24,25} that utilize machine learning methods, for example, deep belief network (DBN) and generalized

regression neural network (GRNN), to predict long-term (seasonal or annual) $\text{PM}_{2.5}$ concentrations using aerosol optical depth (AOD) data. Despite these existing studies, our paper applies machine learning approaches to estimate long-term air quality directly from emissions sources data (i.e., energy use) as well as health co-benefits of fossil energy use and CO_2 emissions for a large country for the first time, providing highly relevant implications for policy making.

Results

Structure and performance of the machine-learning framework

Our novel machine-learning framework applies a modified convolutional neural network architecture (ResCNN) to simulate annual average fine particle ($\text{PM}_{2.5}$) concentration observed by all China’s national-level air-quality monitoring stations in 2015 (1,497 stations in total and 943 are used in the model due to some monitors overlapping in the same grid cell at the geographic resolution we use – $10\text{km} \times 10\text{km}$) from high-resolution fossil energy use data and some additional geographic information. This resolution (100 km^2) is finer than most regional reduced-form models, for example, $1,642\text{ km}^2$ (median) for AP2¹⁶, $1,296\text{ km}^2$ (median) for EASIUR¹⁷, 293 km^2 (population-weighted mean) for InMAP¹⁸, and comparable to some regional comprehensive CTMs, for example, 144 km^2 for many CTMs for the United States¹⁴. We use the most recent year with available data (year 2015) for the analysis in this paper, but the framework could be easily extended to future years and other regions. Specifically, the model output is annual average $\text{PM}_{2.5}$ concentration for each monitoring station collected from China’s National Urban Air Quality Real-time Disclosure Portal²⁶. The model inputs for predicting the annual average $\text{PM}_{2.5}$ concentration of a specific monitoring station are 2D tensors that contain geographical distribution of energy use (by sector and energy type) as well as altitude, temperature, and precipitation in a large surrounding area centered by the station ($610\text{ km} \times 610\text{ km}$, comparable to the domain size used for regional air quality modeling²⁷).

By adopting a standard training process, we select optimal hyper-parameters and correspondingly optimized parameters of the ResCNN framework. We show the prediction performance of our model by comparing the observed and model-predicted concentrations at 943 stations in mainland China for year 2015 (see **Figure 1**). The training set shows the best fit but the validation and test set are also reasonably fitted, suggesting over-fitting is not a major issue. For the test set, mean fractional bias (MFB), mean fractional error (MFE), mean proportional error (MPE), correlation coefficient (ρ), and R square (R^2) are -0.04, 0.12, 0.06, 0.88, and 0.75, respectively, significantly improved compared to the fit of some published reduced-form air quality models (MFB: -0.06, MFE: 0.36, ρ : 0.74, R^2 : 0.13 in Goodkind et al.¹⁴; MPE: 0.37, ρ : 0.62 in Muller¹⁶, see details in **Supplementary Table 2**). The strong predictive power of our model offers us a considerable advantage over conducting the ensuing air quality co-benefits estimation.

We then simulate annual average $\text{PM}_{2.5}$ concentration changes under different policy scenarios with reduced fossil energy use. In this study, we focus on the industrial coal use (including coal use in the power sector), road transportation oil use, and rural and residential coal use (mainly

for heating and cooking), as they are the main targets of energy and environmental policies in China²⁸. For illustration purposes, we first simulate scenarios that curtail fossil energy use in the above sectors by a certain percentage (from 2% to 20% with a step of 2%), respectively. We then estimate population-weighted concentration changes and calculate avoided deaths in each scenario based on most recent concentration-response functions. Although the amount of coal use in the industrial sector is about 40 times higher than rural and residential coal use, the deaths avoided by reducing industrial coal use are only about 4 times higher, suggesting unit pollutant emissions and marginal damage of rural and residential coal use are substantially higher. This result is consistent with the recent finding by Yun et al.²⁹ that China’s residential sector contributed only 7.5% of energy consumption but contributed 27% of primary PM_{2.5} emissions and 23% of the outdoor PM_{2.5} concentrations, respectively. To showcase the computational advantage of our framework, we further downscale the health benefit calculation by estimating marginal damages of fossil fuel use (per ton of coal equivalent) in these sectors by each grid cell (10 km × 10 km). As expected, there is a wide spread of marginal damage of fossil fuel consumption across different sector and also within each sector spatially. We find that reducing rural and residential coal use offers the highest health benefits per ton of use reduction. Further information about the framework is provided in Methods.

Health co-benefits estimations

We first illustrate how our model could be applied in conventional scenario analyses to estimate air quality and health benefits changes with policies aiming to reduce fossil fuel use. We select three key combustion sources in China as our targets, i.e., industrial coal use, rural and residential coal use, and road transportation oil use. **Figure 2** shows the national population-weighted PM_{2.5} concentration and corresponding avoided premature deaths if fossil energy use in one aforementioned sector is curtailed by a certain percentage (from 2% to 20% with a step of 2%), holding other emissions sources and meteorological conditions unchanged. We find the PM_{2.5} concentration decreases and corresponding avoided deaths increase almost linearly with the size of fossil energy curtailment. Annual avoided deaths from reducing 20% of fossil fuels from these three sectors are 55 thousands, 14 thousands, and 3 thousands for industrial coal, rural and residential coal, and road transportation oil, respectively. Avoided deaths from reducing industrial coal and rural and residential coal use have the same order of magnitude, although CO₂ emissions (and energy consumption) from industrial coal use are one order of magnitude higher than emissions from the other two sectors (7.4 gigatons for industrial coal, 0.2 gigatons for rural and residential coal, and 1.0 gigaton for road transportation oil). This result reflects the fact that emissions factor of industrial coal use is significantly lower thanks to strict end-of-pipe measures implemented in China recently, and that locations of emissions sources might be further away from densely-populated areas. While most effective air quality control measures have been targeted at the industrial sector over the past few years²⁸, there are enormous cost-effective potentials to further harvest health benefits from reducing rural and residential coal use.

We then demonstrate how our model could offer estimated spatial distribution of marginal

damage of fossil energy use in different sectors, a task that will require unacceptably long simulation time using conventional CTMs. We show marginal damages attributable to an additional ton of CO₂ emissions from a certain type of fossil energy use at every source location in mainland China in **Figure 3**, with maps for five major air-polluting emissions sources considered in our model (i.e., industrial coal use, rural and residential coal use, coal use in the service sector, road transportation oil use, and industrial oil use). We adopt the value of statistical life (VSL) estimate as 1.8 million in US\$(2015), see Methods for details. Average marginal damage per unit ton of CO₂ emissions ranges from 17 to 360 dollars (US\$ 2015 price) for these sectors, with highest damages for emissions from rural and residential coal use (360 \$/ton) followed by coal use in the service sector (213 \$/ton). Damages for emissions from industrial coal use, road transportation oil and industrial oil use are one order of magnitude lower (23 \$/ton for industrial coal use, 23 \$/ton for industrial oil use, and 17 \$/ton for road transportation oil use). The mean and standard deviation of marginal damages attributable to an additional ton of CO₂ emissions in China are 34 \$/ton and 84 \$/ton, respectively. The mean value has the same order of magnitude compared to the estimate with constant VSL of 1.5 million US\$(2005) in Vandyck et al.⁸. Similar to the pattern found in Goodkind et al.¹⁴, all the distributions are positively skewed, indicating high marginal damages for some hotspots, especially for rural and residential coal use (see **Supplementary Figure 2**). The huge spread across energy use sources and locations reflect substantial differences in coal quality, combustion condition, and end-of-pipe treatment. Overall, the mean marginal damage of CO₂ emissions from coal and oil use in China is 37 and 19 \$/ton, respectively.

Combining estimated marginal damages and fossil energy use data with sectoral and regional source information, we can calculate total damages by sector and by region. For illustration purposes, we aggregate all the mainland Chinese cities into seven regions following the literature^{28,30} and China’s official document³¹: Beijing-Tianjin-Hebei (JJJ representing first characters of three provinces’ short names) and surrounding cities (some cities in Shanxi, Shandong, and Henan province included), Yangtze River Delta provinces (YRD), Pearl River Delta provinces (PRD), other East, other Central, West, and Northeast (the first three regions are China’s major air-pollution control regions). **Figure 4** (a) shows total damages by sector. Industrial coal use has the largest total damage (around \$160 billion), while the total damage of rural and residential coal use is nearly one half of the industrial coal’s total damage. The other types of fossil fuel use have one order of magnitude smaller total damages. **Figure 4** (b) shows total damages with sectoral breakouts by region. As one of the most populous and polluted region, the Beijing-Tianjin-Hebei and surrounding cities bear the highest total damage from fossil fuel emissions (around \$90 billion). Its rural and residential coal use imposes substantially higher total damages than other regions because winter heating contributes much more to the total PM_{2.5} pollution compared to other major air-pollution control regions with less heating demand, e.g., Yangtze River Delta where the total damage is the second highest (around \$60 billion). Some regions show high damages from a specific type of fossil energy use, e.g., industrial oil use in the Northeast, reflecting the relatively concentrated energy use of this type or associated high marginal damage in some hot spots in these regions.

Robustness analysis

We examine the robustness of emissions-concentration relationship derived from our approach by recalculating the average marginal damage using models trained by different sets of hyper-parameters. We select four additional sets of hyper-parameters that produce smallest weighted least square errors on the validation data sets after the set of hyper-parameters chosen for our base-case model. The mean and standard deviation of marginal damage of CO₂ is 35–40 \$/ton and 61–100 \$/ton, which are close to the results from our base-case model (34 \$/ton and 84 \$/ton).

We then evaluate if the selection of surrounding area size for the PM_{2.5} monitoring station could affect the prediction accuracy our framework. Ideally, we should include an area as large as possible to incorporate the impacts of possible long-distance pollutant transportation. In practice, certain thresholds are usually chosen to avoid data availability and computational issues. Besides our base-case model with input tensors representing 610 km × 610 km area centered by a monitor station, we report the prediction accuracy of two alternative models with smaller input tensors (210 km × 210 km and 410 km × 410 km) but identical training process. Surprisingly, models with smaller input tensors can achieve almost similar accuracy compared to our base-case model on the training data set. Our base-case model shows better accuracy on the validation data set, but no significant supremacy on the test data set, see **Supplementary Figure 3**. This result suggests that emissions from a closer surrounding area (210 km × 210 km) dictate the concentration prediction results, and our modeling framework could achieve satisfactory accuracy as long as most relevant input data (fossil energy consumption within a certain distance from the station) are included.

To further illustrate the above finding, we calculate the total damage within different sizes of surrounding area using our base-case model. **Figure 5** shows the total damage caused by emissions within a certain size of square (from 110 km × 110 km to 610 km × 610 km) centered by a monitor station. The total damage curve has a concave relationship with regards to the surrounding area size. Emissions from a faraway source has a smaller impact on the PM_{2.5} concentration of the destination. More than half of the total damage caused by emissions from the full 610 km × 610 km area occur within the centering 210 km × 210 km area (one ninth of the full area). Compared to the results found by Goodkind et al.¹⁴ (half of total PM_{2.5} damages within a 4,096 km radius circle are incurred by people living within 32 km of a source), the total damage curve in China is less concave, possibly because different distributions of pollution sources and population centers that allow the atmospheric transmission to form more local pollution from faraway sources in China.

Discussion

It is well-recognized that marginal damage of emissions and corresponding health benefits of abatement vary widely by place and pollution type. Traditional complicated chemical transport models are not suitable for economic and policy analysis that requires many model iterations to explore the variation of marginal damages. Recent developments of reduced-form models with satisfactory approximations for full-scale models have allowed the researchers to quantify the heterogeneity

of the marginal damage but still place some limitations for broader applications. In this study, we develop a machine-learning based framework that can produce more accurate, accessible, and easy-to-update simulations for air quality, or more specifically, PM_{2.5} concentrations. Applying this framework to estimate the marginal damage of fossil fuel CO₂ emissions by fuel type and source location in China provides us with important insights into future policy designs that aim to achieve ambitious air quality and climate targets.

We find that China’s current carbon pricing stringency does not match the magnitude of marginal damage of per ton of CO₂ emissions. Although many command-and-control climate policies are in place in China, limited market-based instruments have been applied. Currently, only seven regional CO₂ emissions trading schemes (ETS) are in operation with highest average carbon price at the magnitude of \$15/ton in Beijing pilot ETS³², substantially less than the average marginal damage (\$/ton) estimated by this study. We urge a more accelerated development of China’s national ETS to form an appropriate carbon price that can better internalize the public health externality of CO₂ emissions.

The highly heterogeneous marginal damage by fuel type and location has also important implications. By far, only CO₂ emissions from industrial fossil fuel use are planned to be covered by China’s national ETS³³. Our analysis has shown, however, CO₂ emissions from industrial fossil fuel have a much lower marginal damage compared to the emissions from coal use in the rural and residential as well as service sector. Therefore, complementary policies that place an effective carbon price on these sectors to encourage fuel switching (e.g., coal to natural gas for small boilers or electrification of residential heating) are essential. We also note that the marginal damage of CO₂ emissions in more populous eastern China, particularly in the North China Plain and Yangtze River Delta region, is much higher than that of emissions in the rest of the country, suggesting a trading ratio³⁴ could be considered in the future design of China’s national ETS.

Applying machine learning techniques in the environmental integrated assessment motivates fruitful future work. Although our framework provides satisfactory results for the annual PM_{2.5} concentration estimation, prediction accuracy for pollutants other than particular matters needs further improvement. **Supplementary Figure 4** shows the prediction accuracy for PM₁₀, SO₂, NO₂, CO, and O₃ by applying the same framework and training process to these pollutants. Accuracy of PM₁₀ is similar to that of PM_{2.5}. For SO₂, NO₂, and CO, the framework can achieve acceptable fitting results on the training data set but fail to achieve consistent accuracy on the validation and test data sets; the fitness is low even on the training data set for ozone. Refining the framework architecture and training process and incorporating relevant atmospheric condition data for pollutants other than particular matters remains an interesting direction for future research.

We believe it is important to extend the co-benefits analysis implemented in our study to more developing countries with imperative air pollution control and climate mitigation policy development. High-resolution marginal damage estimations that are very relevant for policy making have been almost exclusively conducted in the United States^{9–15}, suggesting the complexity of the methodology even with elaborately-designed reduced-form CTMs. We hope our machine learning framework would supply a more accessible tool for researchers and policymakers to implement more

comprehensive and timely analysis in more developing countries that are constrained with emissions inventory and atmospheric measurement data.

Methods

Methods, including statements of data availability and references, are available in the online version of this paper.

References

- 1 McCollum D. L. et al. Climate policies can help resolve energy security and air pollution challenges. *Clim. Change* **119**, 479–494 (2013).
- 2 West J. J. et al. Co-benefits of global greenhouse gas mitigation for future air quality and human health. *Nat. Clim. Change* **3**, 885–889 (2013).
- 3 Thompson T. M., Rausch S., Saari R. K. & Selin N. E. A systems approach to evaluating the air quality co-benefits of US carbon policies. *Nat. Clim. Change* **4**, 917–923 (2014).
- 4 Driscoll T. C. et al. US power plant carbon standards and clean air and health co-benefits. *Nat. Clim. Change* **5**, 535–540 (2015).
- 5 Shindell D. T., Lee Y. & Faluvegi G. Climate and health impacts of US emissions reductions consistent with 2°C. *Nat. Clim. Change* **6**, 503–507 (2016).
- 6 Li M. et al. Air quality co-benefits of carbon pricing in China. *Nat. Clim. Change* **8**, 398–403 (2018).
- 7 Shindell D. T., Faluvegi G., Seltzer K. & Shindell C. Quantified, localized health benefits of accelerated carbon dioxide emissions reductions. *Nat. Clim. Change* **8**, 291–295 (2018).
- 8 Vandyck T. et al. Air quality co-benefits for human health and agriculture counterbalance costs to meet Paris Agreement pledges. *Nat. Commun.* **9**, 4939 (2018).
- 9 Mayfield E. N. et al. Cumulative environmental and employment impacts of the shale gas boom. *Nat. Sustain.* **2**, 1122–1131 (2019).
- 10 Dedoussi I. C., Eastham S. D., Monier E. & Barrett S. R. H. Premature mortality related to United States cross-state air pollution. *Nature* **578**, 261–265 (2020).
- 11 Muller N. Z. & Mendelsohn R. Efficient pollution regulation: Getting the prices right. *Am. Econ. Rev.* **99**(5), 1714–1739 (2009).
- 12 Holland S. P., Mansur E. T., Muller N. Z. & Yates A. J. Are there environmental benefits from driving electric vehicles? The importance of local factors. *Am. Econ. Rev.* **106**(12), 3700–3729 (2016).

- 13 Tessum C. W. et al. Inequity in consumption of goods and services adds to racial–ethnic disparities in air pollution exposure. *Proc. Natl. Acad. Sci. U.S.A.* **116**(13), 6001–6006 (2019).
- 14 Goodkind A. L. et al. Fine-scale damage estimates of particulate matter air pollution reveal opportunities for location-specific mitigation of emissions. *Proc. Natl. Acad. Sci. U.S.A.* **116**(18), 8775–8780 (2019).
- 15 Hill J. et al. Air-quality-related health damages of maize. *Nat. Sustain.* **2**, 397–403 (2019).
- 16 Muller N. Z. Linking policy to statistical uncertainty in air pollution damages. *B. E. J. Econ. Anal. Pol.* **11**(1), Article 32 (2011).
- 17 Heo J., Adams P. J. & Gao H. O. Public health costs of primary PM and inorganic PM precursor emissions in the United States. *Environ. Sci. Technol.* **50**(11), 6061–6070 (2016).
- 18 Tessum C. W., Hill J. D. & Marshall J. D. InMAP: A model for air pollution interventions. *PLOS One* **12**(4), e0176131 (2017).
- 19 Van Dingenen R. et al. TM5-FASST: a global atmospheric source-receptor model for rapid impact analysis of emission changes on air quality and short-lived climate pollutants. *Atmos. Chem. Phys.* **18**, 16173–16211 (2018).
- 20 Ong B. T., Sugiura K. & Zettsu K. Dynamically pre-trained deep recurrent neural networks using environmental monitoring data for predicting PM_{2.5}. *Neural. Comput. & Applic.* **27**, 1553–1556 (2016).
- 21 Kerckhoffs J. et al. Performance of prediction algorithms for modeling outdoor air pollution spatial surfaces. *Environ. Sci. Technol.* **53**(3), 1413–1421 (2019).
- 22 Xing J. et al. Deep Learning for Prediction of the Air Quality Response to Emission Changes. *Environ. Sci. Technol.* **54**(14), 8589–8600 (2020).
- 23 Kelp M. et al. Toward stable, general machine-learned models of the atmospheric chemical system. *EarthArXiv* <https://doi.org/10.31223/osf.io/8vy6j> (2020).
- 24 Li T. et al. Point-surface fusion of station measurements and satellite observations for mapping PM_{2.5} distribution in China: Methods and assessment. *Atmos. Environ.* **152**, 477–489 (2017).
- 25 Li T. et al. Estimating ground-level PM_{2.5} by fusing satellite and station observations: A geointelligent deep learning approach. *Geophys. Res. Lett.* **44**(23), 11,985–11,993 (2017).
- 26 China’s National Urban Air Quality Real-time Disclosure Portal; <http://106.37.208.233:20035/>
- 27 Zhang F. et al. The characteristics of air pollution episodes in autumn over the southern Hebei, China. *World J. Eng.* **12**(3), 221–236 (2015).

- 28 Zhang Q. et al. Drivers of improved PM_{2.5} air quality in China from 2013 to 2017. *Proc. Natl. Acad. Sci. U.S.A.* **116**(49), 24463–24469 (2019).
- 29 Yun X. et al. Residential solid fuel emissions contribute significantly to air pollution and associated health impacts in China. *Sci. Adv.* **6**: eaba7621 (2020).
- 30 Liang X. et al. Air quality and health benefits from fleet electrification in China. *Nat. Sustain.* **2**, 962–971 (2019).
- 31 National Bureau of Statistics. Definitions of the East, West, Central, and Northeast region in China; http://www.stats.gov.cn/ztjc/zthd/sjtjr/dejtkjfr/tjkp/201106/t20110613_71947.htm (2011).
- 32 The World Bank. Carbon Pricing Dashboard; https://carbonpricingdashboard.worldbank.org/map_data (2020).
- 33 Pizer W. A. & Zhang X. China’s new national carbon market. *AEA P&P* **108**, 463–467 (2018).
- 34 Holland S. P. & Yates A. J. Optimal trading ratios for pollution permit markets. *J. Pub. Econ.* **125**, 16–27 (2015).

Correspondence and requests for materials should be addressed to Shenhao Wang and Bofeng Cai (E-mail: shenhao@mit.edu and caibf@caep.org.cn).

Acknowledgments

We acknowledge the support of the National Science Foundation of China (Project No. 71690244). Da Zhang has been supported by the MIT Joint Program on the Science and Policy of Global Change, funded through a consortium of industrial sponsors and Federal grants, including the U.S. Department of Energy (DOE) under Integrated Assessment Grant (DE-FG02-94ER61937). We thank Jiacheng Cui and Xinhao Wang for their excellent research assistance.

Author contributions

D.Z., B.C., and S.W. conceived the research. D.Z., Q.W., and S.W. performed the modeling simulations. All authors discussed the results and contributed to the writing of the paper.

Competing financial interests

The authors declare no competing financial interests.

Methods

Data sets and preprocessing. We denote the inputs used to predict annual average fine particle ($\text{PM}_{2.5}$) concentration as $x_{ijkn} \in \mathbb{R}^4$ with four indices: n is the index of air-quality monitoring stations ($1 \leq n \leq N$); k is the index of different types of data inputs that are used for the prediction, including the level of fossil energy use of a specific energy type in a specific sector as well as some additional geographic information, for example, altitude, temperature, and precipitation ($1 \leq k \leq K$); and (i, j) is the location index representing a grid cell of an area centered around the station ($1 \leq i, j \leq I, J$). Therefore, x_{ijkn} represents the value of a specific input k for a grid cell (i, j) that is close to a specific station n . The total number of stations is $N = 943$. We include eight ($K = 8$) types of data inputs for each station in the form of 2D tensors (I, J) . Specifically, these eight types of data inputs are: (1) rural and residential coal use (RRC), (2) industrial coal use (IDC), (3) industrial oil use (IDO), (4) coal use in service industry (SVC), (5) oil use in road transportation (TRN), (6) altitude (ALT), (7) annual average temperature (TEM), and (8) annual average precipitation (PCP). The number of pixels in each 2D tensor in our main model specification is $I \times J = 61 \times 61$. With each pixel representing a $10 \text{ km} \times 10 \text{ km}$ cell, the geographical size of each 2D tensor equals to $[I \times 10] \times [J \times 10] = 610 \text{ km} \times 610 \text{ km}$. The large geographical coverage of each station, along with 943 stations in total, guarantees that our analysis covers all the territory of mainland China with permanent residents.

The output of our main model is the annual average PM_{2.5} concentration, denoted as y_n . Note that each $y_n \in \mathbb{R}$ is a real number for each station, different from the high dimensionality of the input variable x_{ijkn} . We also train separate models to predict annual average concentrations of other air pollutants, including the annual average concentration of PM_{2.5}, PM₁₀, SO₂, NO₂, CO, and O₃. While the output of the models are different, the model structure and training process are similar to our main model specification.

Inputs x_{ijkn} are normalized before modeling to improve prediction accuracy and facilitate training process³⁵. The input x_{ijkn} is normalized as following:

$$x_{ijkn} \leftarrow \frac{x_{ijkn} - \bar{x}_{kn}}{\sigma_{kn}} \quad [1]$$

in which

$$\bar{x}_{kn} = \frac{1}{IJ} \sum_{i=1, j=1}^{I, J} x_{ijkn}; \quad \sigma_{kn} = \sqrt{\frac{1}{IJ} \sum_{i=1, j=1}^{I, J} (x_{ijkn} - \bar{x}_{kn})^2} \quad [2]$$

For stations that are close to national boundaries or sea, the 2D tensors could have cells that we do not have energy use information. We fill these cells with zeros.

ResCNN model architecture. As visualized in **Supplementary Figure 1**, our model architecture consists of two parts. The upper part is a standard AlexNet³⁶, which uses the normalized 3D tensor x_{ijkn} as input for each station n . It starts with repeated blocks of convolutional layers and max pooling layers, and ends with several fully connected layers. The bottom part is similar to linear regression that uses linear specification and average value of each 1D tensor \bar{x}_{kn} as input. The two parts provide complementary information: AlexNet absorbs the nonlinear structural spatial information of each 3D tensor, while the linear part absorbs the magnitude information of each 3D tensor, which is lost in AlexNet due to normalization. Intuitively, PM_{2.5} concentration varies with the average amount of the energy use (e.g., higher fossil energy use usually causes higher pollution concentration), and it also depends on some spatial structural information which is missing in the average values (e.g., fossil energy use that is closer to the station will have a larger effect on the concentration, and the spatial distribution of one type of fossil energy use may have a nonlinear interaction with the spatial distribution of another type of fossil energy use). Different from the traditional process of explicitly specifying the nonlinear relationship, our model automatically learns the nonlinear relationship between energy consumption, atmospheric conditions, geographic information, and resulting annual average concentration level of PM_{2.5}. The synthesis of the AlexNet and the linear parts is similar to ResNet³⁷, which is also a linear combination of linear and nonlinear feature maps. We therefore name the model architecture as ResCNN because it combines linear regression to capture the magnitude effect and CNN to capture the residual nonlinear relationship. Mathematically, the ResCNN model is

$$y_n = f(x) = f_c(x_{ijkn}) + f_l(\bar{x}_{kn}) = (g_L \circ g_{L-1} \circ \dots \circ g_1)(x_{ijkn}) + w'_K \bar{x}_{kn} \quad [3]$$

In Equation 3, $(g_L \circ g_{L-1} \circ \dots \circ g_1)(x_{ijkn})$ represents the AlexNet architecture with L layers; $w'_K \bar{x}_{kn}$ represents the linear part.

Evaluation Metrics. To evaluate the performance of the ResCNN, we have adopted some common evaluation metrics for the performance of the CTMs, for example, coefficient of determination (R^2), normalized mean bias (NMB), and normalized mean error/mean absolute percentage error (NME/MAPE), from the literature^{16,18,19,38,39}. We add an important modification to all of the evaluation metrics by introducing normalized weights w_n that are proportional to the population that a specific station n corresponds to. For example, if there is only one station that enters our sample for a specific city, we assume the station generates the concentration reading that represents the exposure of the city’s whole population; however, if multiple stations are present in our sample for a city, we assume each station generates the concentration reading that represents an equal share of the city’s population. With this modification, the performance measure gives more weights on the prediction accuracy of stations corresponding to larger population because the marginal damage we estimate later is in proportional to the population. We illustrate all the metrics we compute in **Supplementary Table 1**. Our main model uses the weighted least square errors on the validation set in hyper-parameter searching, which we discuss in the section below.

Hyper-Parameter searching and training. To address the challenge of specifying the appropriate hyper-parameters, this study combines random search and grid search. First, random searches (400 trials) in a pre-specified, larger hyper-parameter space are done. Conditioning on each hyper-parameter and while keeping the others random, hyper-parameter values that yield consistently lower performance or higher variance in performance are pruned. Then a complete grid search was done to the remaining hyper-parameter values (384 combinations). While numerous methods can be used to identify the best hyper-parameter, the simple random search⁴⁰ is still a useful benchmark, even in comparison to more complicated hyper-parameter searching methods based on reinforcement learning or Gaussian process^{41–43}. The full hyper-parameter space is shown in **Supplementary Table 2**, and the pruned hyper-parameter space is shown in **Supplementary Table 3**. Among the hyper-parameters, some are model specific and require some searching in each specific application. For instance, dropout and batch normalization were found as effective regularization in several studies^{44,45}. Data augmentation⁴⁶ assumes the invariance property: when images are rotated or flipped, the new images should not change the predicted values \hat{y} . On the other hand, some hyper-parameters are set to follow the common practice. For instance, Rectified Linear Unit (ReLU) is used as activation functions for each neuron; He initialization⁴⁷ is used to address the problem of vanishing and exploding gradients; Adam optimizer⁴⁸ is used for gradient descent optimization.

The ResCNN model is trained by empirical risk minimization (ERM). Formally,

$$\min_W E(W; W_h) = \min_W \frac{1}{N} \sum_{n=1}^N w_n \times (y_n - f(x_{ijkn}; W, W_h))^2 \quad [4]$$

in which W represents parameters and W_h represents hyper-parameters, while w_n represents the weight of each observation as we describe in the above section. Note that the training in Equation

4 is conditioning on the specific choice of hyper-parameters W_h . Denote $W^* = \underset{W}{\operatorname{argmin}} E(W; W_h)$, the optimum hyper-parameter W_h^* is chosen by random searching:

$$W_h^* = \underset{W_h \in W_h^{(1)}, W_h^{(2)}, \dots, W_h^{(S)}}{\operatorname{argmin}} E(W^*; W_h) \quad [5]$$

W_h^s represents random sample from the hyper-parameter space. The best hyper-parameter W_h^* is chosen out of $S = 100$ training. To train model and choose hyper-parameters, the full dataset is split into training, validation, and testing sets with the ratio equals to 3 : 1 : 1. The training set is used to train ResCNN model as in Equation 4; validation set is used for the selection of hyper-parameter as in Equation 5; testing set is used for model evaluation and comparison.

Health impacts and valuation We apply the up-to-date GEMM NCD+LRI method⁴⁹ to estimate avoided premature death related to reductions in chronic exposure to outdoor fine particulate matter (PM_{2.5}) under different scenarios. The GEMM NCD+LRI method is considered as a major update to the widely-used IER 5-COD approaches^{50,51} and has been adopted in some recent cost-benefit analysis^{10,28,30}. Compared to the IER approach, the GEMM NCD+LRI method incorporates findings from recent cohort studies that quantify the relationship between avoided premature death and ambient PM_{2.5} concentration (C-R relationship) in regions with high PM_{2.5} concentration levels, making it more appropriate to be applied in relatively more polluted countries like China. In addition, the GEMM NCD+LRI method associates PM_{2.5}-related death to non-accidental deaths caused by noncommunicable diseases and lower respiratory infections, a more comprehensive range than the five specific causes of death considered in the IER 5-COD approaches.

The GEMM NCD+LRI quantifies the relationship between hazard ratio (RR) of NCD+LRI and ambient PM_{2.5} concentration (c) with the following equation:

$$RR(c) = \exp\left(\theta \times \frac{\ln\left(\frac{\max(0, c - c_f)}{\alpha} + 1\right)}{1 + \exp\left(-\frac{\max(0, c - c_f) - \mu}{\nu}\right)}\right) \quad [6]$$

where θ , α , μ , ν and c_f are all shape parameters that define the C-R relationship. Since the baseline mortality rate is different for adults with different ages, we follow the convention to divide population in a specific grid cell n into 12 subgroups (adults with age from 25 to 85 and above in five-year intervals). Consider two scenarios (scenario 0 and scenario 1) with different ambient PM_{2.5} concentration levels (c_0, c_1), the avoided death under scenario 1 compared to scenario 0 in grid cell n is calculated by summing up avoided deaths of all m age groups:

$$\Delta M_n = \sum_m M_m^B \times \text{pop}_{m,n} \times \left(\frac{1}{RR(c_{1,n})} - \frac{1}{RR(c_{0,n})} \right) \quad [7]$$

where M_m^B is the baseline mortality rate for age group m in China, retrieved from the Global Health Data Exchange, and $\text{pop}_{m,n}$ is the population of age group m in grid cell n .

We adopt the assumption that θ has a normal distribution with mean μ_θ and standard deviation σ_θ ⁵⁰. We can then sample 1,000 points from the normal distribution and calculate the mean and 95% confidence interval of avoided death using Equation 7. An alternative faster approach to obtain the mean avoided death $\overline{\Delta M_n}$ is to use the following equation to first calculate the mean of $1/RR(c_n)$, which has a lognormal distribution,

$$\overline{1/RR(c_n)} = \exp(-\mu_\theta \frac{\ln(\frac{\max(0, c_n - c_f)}{\alpha} + 1)}{1 + \exp(-\frac{\max(0, c_n - c_f) - \mu}{v})}) + \frac{1}{2} (\sigma_\theta \frac{\ln(\frac{\max(0, c_n - c_f)}{\alpha} + 1)}{1 + \exp(-\frac{\max(0, c_n - c_f) - \mu}{v})})^2 \quad [8]$$

and then calculate the mean avoided death $\overline{\Delta M_n}$.

$$\overline{\Delta M_n} = \sum_m M_m^B \times \text{pop}_{m,n} \times (\overline{1/RR(c_{1,n})} - \overline{1/RR(c_{0,n})}) \quad [9]$$

In our scenario analysis, where sector k' emission is curtailed by p (p ranges from 2% to 20%), $c_{0,n}$ is taken to be the predicted baseline PM_{2.5} concentration, and $c_{1,n}$ is obtained by reducing all input emissions in sector k' by p :

$$c_{1,n} = f(x_{ijkn, k \neq k'}, x_{ijk'n} * (1 - p); W^*, W_h^*) \quad [10]$$

The marginal change of PM_{2.5} due to the marginal change of emissions can be obtained from the gradients of PM_{2.5} with respect to the input emissions from each sector and each grid cell ($\frac{\partial y}{\partial x_{ijk}}$). Since back propagation is used for training the neural network, the gradients can be directly exported from the models. For each unit emissions increase in sector k' in cell i, j , the mean avoided death for station n is:

$$\overline{\Delta M_{ijk'n}} = \sum_m M_m^B \times \text{pop}_{m,n} \times \left[\overline{1/RR\left(c_{0,n} + \frac{\partial y_n}{\partial x_{ijk'n}}\right)} - \overline{1/RR(c_{0,n})} \right] \quad [11]$$

where again $c_{0,n}$ is taken to be the predicted baseline PM_{2.5} concentration.

We close the estimate of marginal monetary damages related to increased premature mortality due to an additional ton of CO₂ emissions by using an inferred value of statistical life (VSL) for China based on the U.S. EPA recommended VSL of 8.7 million in US\$(2015)⁵². We adopt the income elasticity for high-income countries recommended by a recent meta-study⁵³ for extrapolating from the U.S. VSL (VSL_{base}) to the VSL for China (VSL):

$$VSL = VSL_{base} \times (\text{pcGDP}_{China} / \text{pcGDP}_{U.S.})^{0.8} \quad [12]$$

where pcGDP_{China} and $\text{pcGDP}_{U.S.}$ represent GDP per capita in 2015 for China and the U.S., respectively. Equation 12 gives the VSL estimate as 1.8 million in US\$(2015) for China.

Combining the considerations of premature mortality and the inferred value of statistical life, the marginal monetary damages due to an additional ton of CO₂ emissions in sector k' in cell i, j is

$$MD_{ijk'} = - \sum_n VSL \times \overline{\Delta M_{ijk'n}} \quad [13]$$

The total monetary damages incurred by emissions from sector k' are the sum of the production of marginal monetary damages and emissions in each cell:

$$TD_{k'} = \sum_{i,j} MD_{ijk'} \times x_{ijk'} \quad [14]$$

Data availability The scripts and data that support the findings of this study are available online (web address to be announced).

References

- 35 Hinton G. E. et al. Improving neural networks by preventing co-adaptation of feature detectors. *ArXiv Preprint*, arXiv:1207.0580 (2012).
- 36 Krizhevsky A., Sutskever I., & Hinton G. E. Imagenet classification with deep convolutional neural networks. *Adv. Neural. Inf. Process. Syst.*, 1097–1105 (2012).
- 37 He K. et al. Deep residual learning for image recognition. *Proceedings of the IEEE Conference on Computer Vision and Pattern Recognition*, 770–778 (2016).
- 38 Appel K. W. et al. Examination of the Community Multiscale Air Quality (CMAQ) model performance over the North American and European domains. *Atmos. Environ.* **13**, 142–155 (2012).
- 39 Zhong M. et al. Air quality modeling with WRF-Chem v3.5 in East Asia: Sensitivity to emissions and evaluation of simulated air quality. *Geosci. Model Dev.* **9**, 1201–1218 (2016).
- 40 Bergstra J. & Bengio Y. Random search for hyper-parameter optimization. *J. Mach. Learn. Res.* **13**, 281–*Geosci. Model Dev.* **9**, 1201–1218 (2016).
- 41 Zoph B. & Le Q. V. Neural architecture search with reinforcement learning. *ArXiv Preprint*, arXiv:1611.01578 (2016).
- 42 Zoph B. et al. Learning transferable architectures for scalable image recognition. *ArXiv Preprint*, arXiv:1707.07012 (2017).
- 43 Snoek J. et al. Scalable Bayesian optimization using deep neural networks. *International Conference on Machine Learning*, 2171–2180 (2015).
- 44 Srivastava N. et al. Dropout: a simple way to prevent neural networks from overfitting. *J. Mach. Learn. Res.* **15**, 1929–1958 (2014).

- 45 Ioffe S. & Szegedy C. Batch normalization: Accelerating deep network training by reducing internal covariate shift. *International Conference on Machine Learning*, 448–456 (2015).
- 46 Goodfellow I. Deep learning. *MIT Press*, (2016).
- 47 Géron A. Hands-on machine learning with Scikit-Learn and TensorFlow: concepts, tools, and techniques to build intelligent systems. *O’Reilly Media, Inc.*, (2017).
- 48 Kingma D. P. & Ba J. Adam: A method for stochastic optimization. *ArXiv Preprint*, arXiv:1412.6980 (2014).
- 49 Burnett R. T. et al. Global estimates of mortality associated with longterm exposure to outdoor fine particulate matter. *Proc. Natl. Acad. Sci. U.S.A.* **115**(38), 9592–9597 (2018).
- 50 Burnett R. T. et al. An Integrated Risk Function for Estimating the Global Burden of Disease Attributable to Ambient Fine Particulate Matter Exposure. *Environ. Health Perspect.* **122**, 397–403 (2014).
- 51 Cohen A. J. et al. Estimates and 25-year trends of the global burden of disease attributable to ambient air pollution: An analysis of data from the Global Burden of Diseases Study 2015. *Lancet* **389**(10082), 1907–1918 (2017).
- 52 U.S. Environmental Protection Agency. Guidelines for Preparing Economic Analyses (U.S. EPA Office of the Administrator, Washington, DC), Technical Report EPA 240-R-10-001 (2010).
- 53 Robinson L. A. et al. Valuing mortality risk reductions in global benefit-cost analysis. *J. Benefit Cost Anal.* **10**(S1), 15–50 (2014).

Figure Captions

Figure 1 Comparison of model-predicted and observed $PM_{2.5}$ concentrations at 943 stations in mainland China for year 2015 by training, validation, and test data sets.

Figure 2 China’s population-weighted $PM_{2.5}$ concentrations and corresponding avoided deaths (shaded areas represent 95% confidence intervals) in 2015 if fossil energy use in a polluting sector were curtailed by a certain percentage (from 2% to 20%).

Figure 3 Marginal damages measured in dollars attributable to an additional ton of CO_2 emissions from (a) rural and residential coal use, (b) coal use in the industry sector, (c) oil use in the industry sector, (d) coal use in the service sector, and (e) oil use in the transportation sector.

Figure 4 Total damages from fossil fuel use in China (a) by sector and (b) by region with sectoral breakouts.

Figure 5 Total damage by distance (measured by the edge length of the square centered at a monitor station) and emissions source type.

Figures

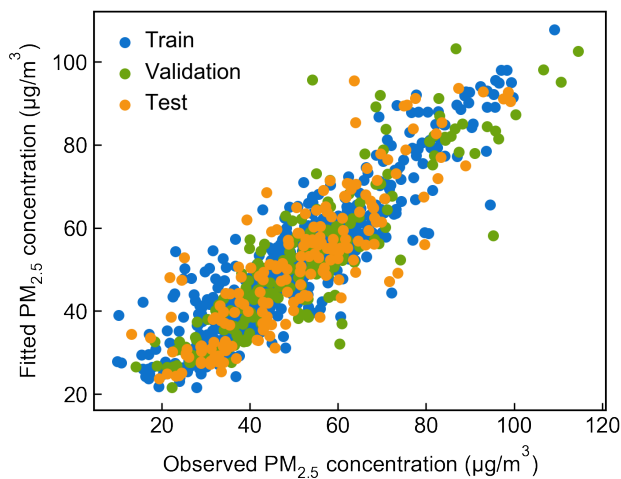


Figure 1: Comparison of model-predicted and observed PM_{2.5} concentrations at 943 stations in mainland China for year 2015 by training, validation, and test data sets.

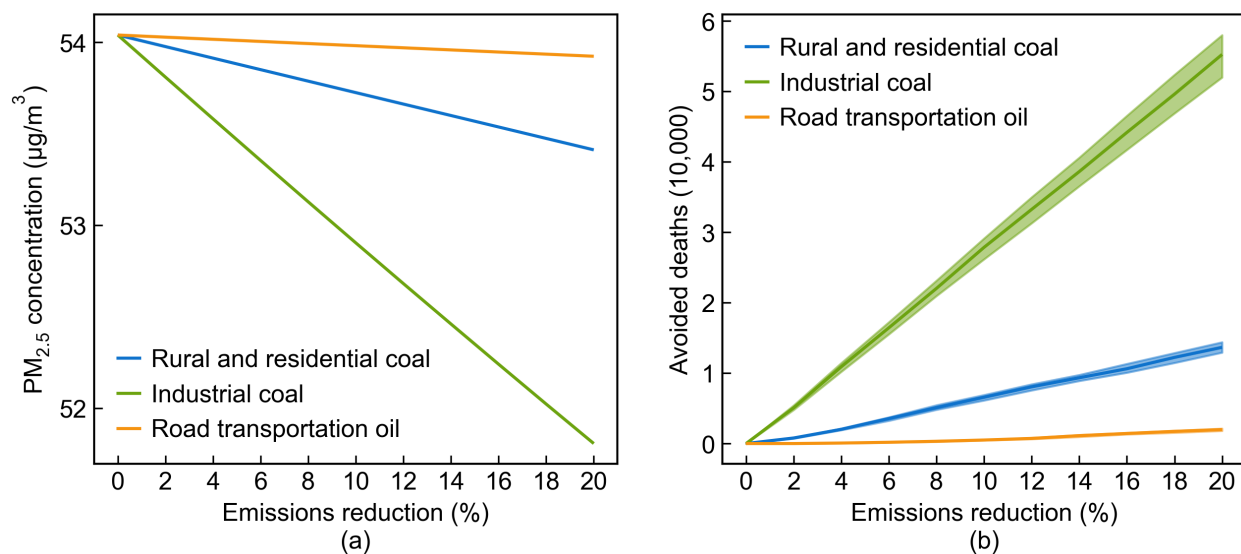


Figure 2: China's population-weighted PM_{2.5} concentrations and corresponding avoided deaths (shaded areas represent 90% confidence intervals) in 2015 if fossil energy use in a polluting sector were curtailed by a certain percentage (from 2% to 20%).

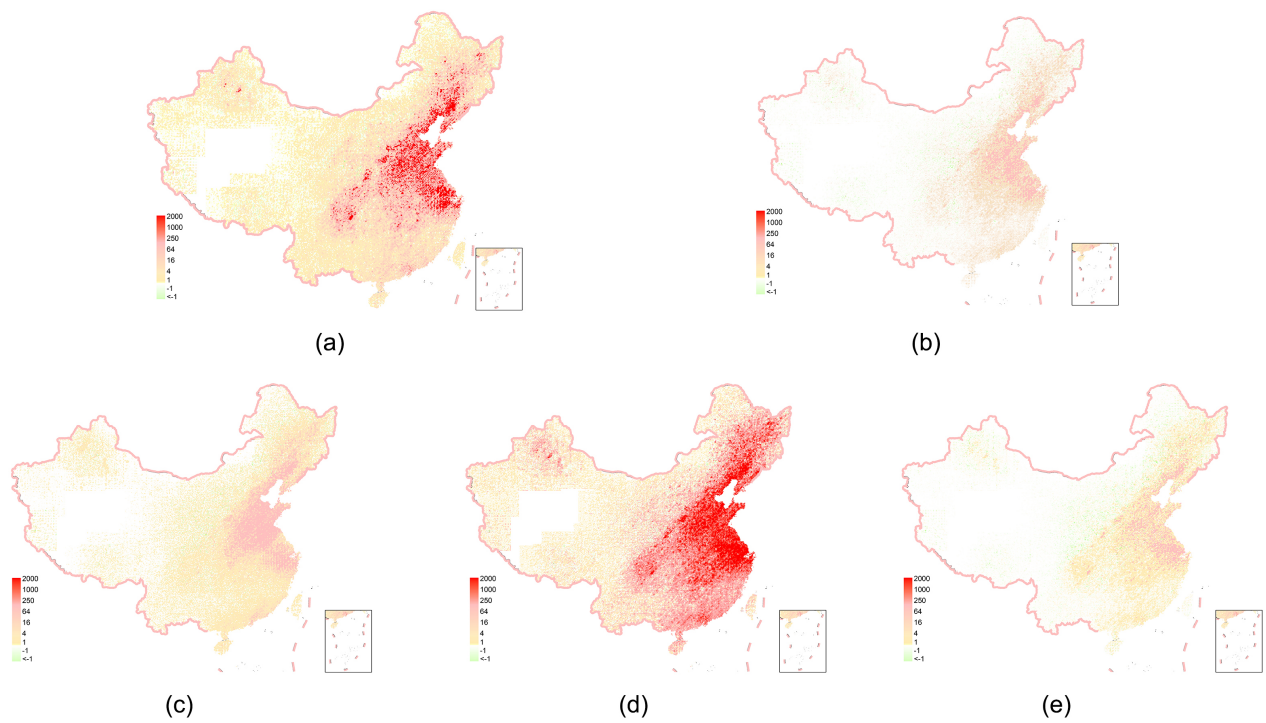
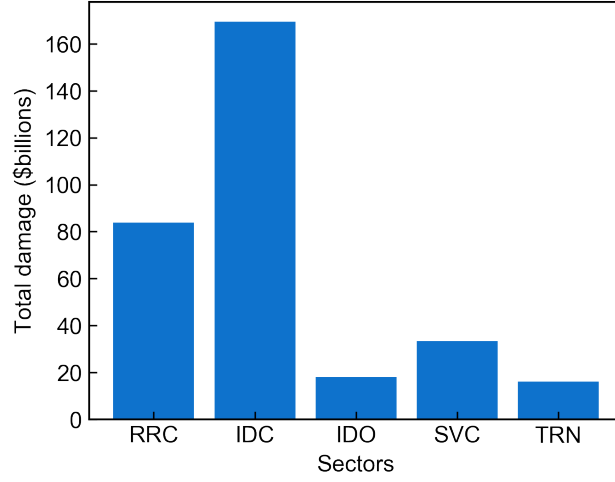
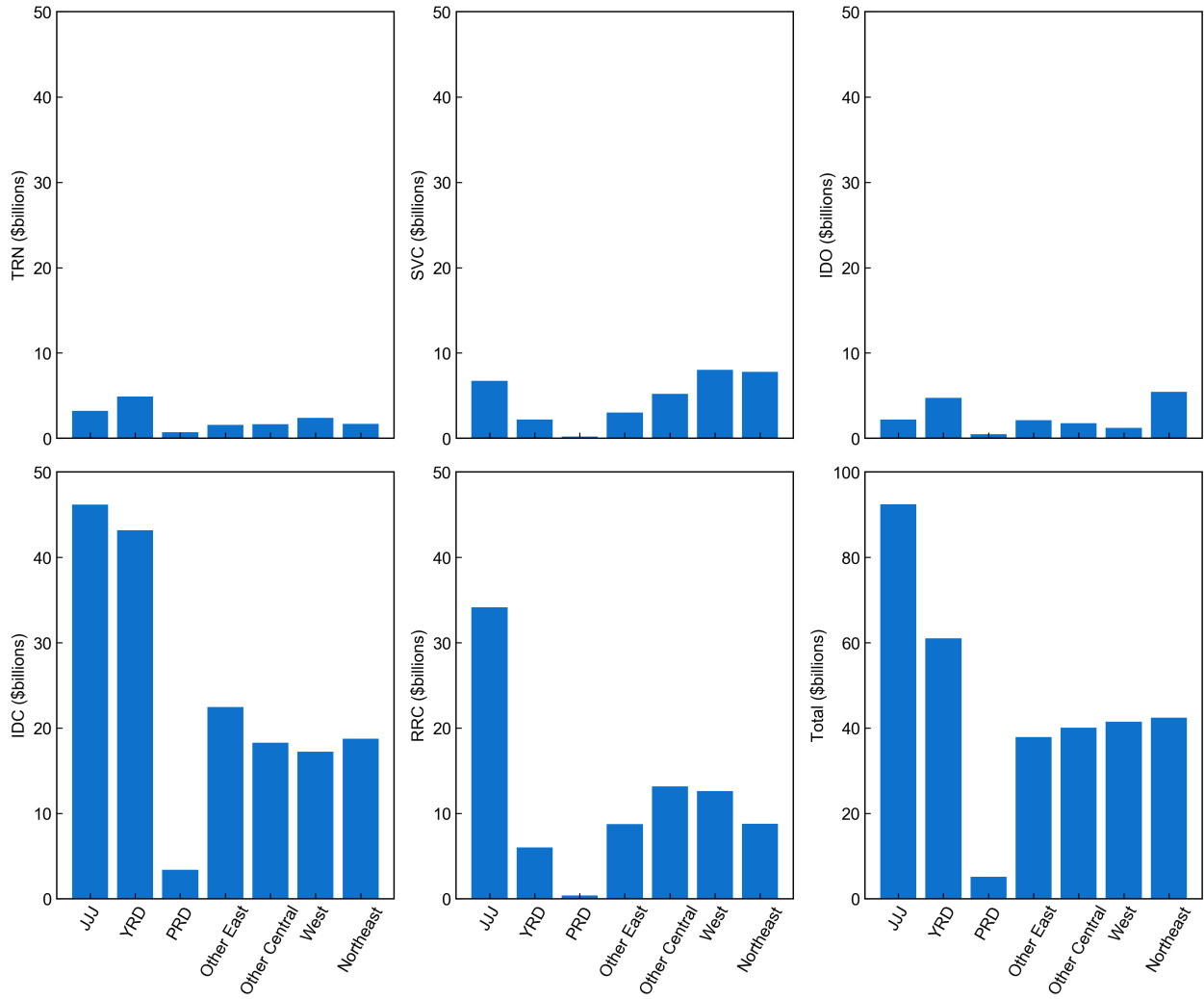


Figure 3: Marginal damages measured in dollars attributable to an additional ton of CO₂ emissions from (a) rural and residential coal use, (b) coal use in the industry sector, (c) oil use in the industry sector, (d) coal use in the service sector, and (e) oil use in the transportation sector.



(a)



(b)

Figure 4: Total damages from fossil fuel use in China (a) by sector and (b) by region with sectoral breakouts.

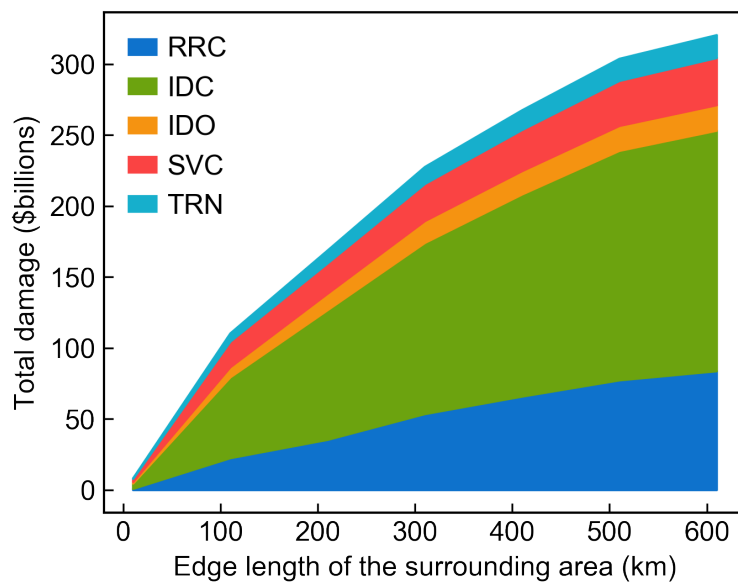


Figure 5: Total damage by distance (measured by the edge length of the square centered at a monitor station) and emissions source type.